TELKOMNIKA, Vol.16, No.3, June 2018, pp. 1027~1033
ISSN: 1693-6930, accredited **A** by DIKTI, Decree No: 58/DIKTI/Kep/2013
DOI:10.12928/TELKOMNIKA.v16i3.6756

Voltage Oriented Decoupled Control Scheme for DFIG's Grid Side Converter

S.A. Kamran*, Javier Muñoz
Department of Industrial Technologies Universidad de Talca, Talca, Chile, Pakistan
*Corresponding author, e-mail: kame7970@yahoo.com

Abstract

This paper proposes a novel voltage oriented decoupled control scheme for the DFIG's Grid Side Converter (GSC) of a 2.3Mw, 690V, 50Hz, 6 pole doubly-fed induction generator (DFIG) based wind generation system. For Rotor Side Converter (RSC), slip and constant V/Hz control scheme along with a feedback control via PWM is selected but not explained in this paper.Based on the per-phase steady state equivalent circuit model of a DFIG, relationship between stator and rotor voltages is developed. Voltage oriented decoupled control scheme for GSC is designed in such a way that it can keep the dc link voltage constant by regulating grid reactive power when required. The space vector modulation (SVM) algorithm is explained breifly and implemented for the two-level GSC. MATLAB/SIMULINK (R2015a) software validates the proposed control scheme for GSC.

Keywords*: Doubly-fed induction generator-modeling, space vector modulation (SVM) algorithm, grid-side converter, voltage oriented decoupled control*

1. Introduction

Conventional energy sources generate energy at a constant rate while renewable fluctuate with the variability in the natural sources from which they derive energy. Such fluctuations are particularly acute for wind and solar photovoltaics. Due to the fluctuating nature of wind power, it is advantageous to operate the WTG at variable speed which reduces the physical stress on the turbine blades and drive train, and which improves system aerodynamic efficiency and torque transient behaviors [1]. Conventional power generation utilizes synchronous machines, modern wind power systems use induction machines extensively in wind turbine applications.

These induction generators fall into two types: fixed speed induction generators (FSIGs) with squirrel cage rotors [2] and doubly fed induction generators (DFIGs) with wound rotors [3].The DFIG is currently the system of choice for multi-MW wind turbines as over 85% of the installed wind turbines utilize DFIGs .In the DFIG topology, the stator is directly connected to the grid through transformers and the rotor is connected to the grid through PWM power converters. The converters can control the rotor circuit current, frequency and phase angle shifts. As shown in Figure 1, the rotor of the DFIG is mechanically connected to the wind turbine through a drive train system, which may contain high and low speed shafts, bearings and a gearbox. The rotor is fed by the bi-directional voltage-source converters. Thereby, the speed and torque of the DFIG can be regulated by controlling the rotor side converter (RSC) [4]-[6].

Taking into account the only one converter within a DFIG system. This paper is organized as follows. Section II describes the DFIG mathematical modeling. To analyze the DFIG's performance, its per-phase equivalent circuit for steady state operation is analyzed and relationships between stator and rotor voltages are developed. In section III, operation of GSC with VOC and reactive power control are illustrated in detail. Brief principle and implementation of SVM algorithm for the two-level GSC is explained in section IV. Simulation results on a 2.3MW DFIG system are provided in section V and finallysection VI draws the conclusions.

Received July 10, 2017; Revised January 8, 2018; Accepted May 12, 2018

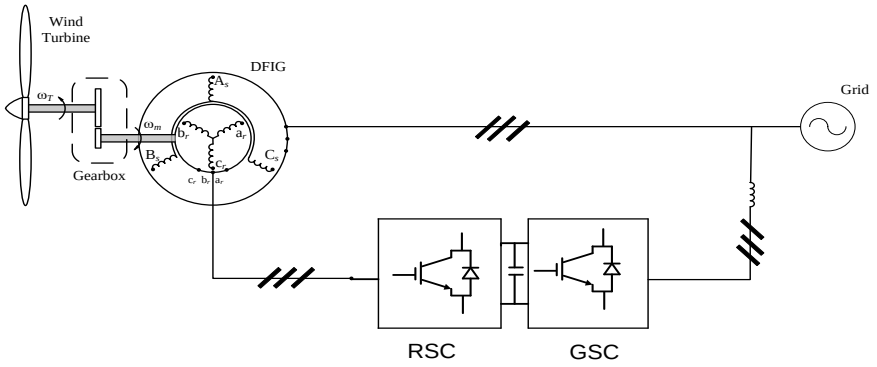

Figure 1. The conventional configuration of DFIG-WT

2. DFIG's mathematical modeling

To determine DFIG's performance under steady-state operation, its per-phase equivalent model is selected and shown in Figure 2.

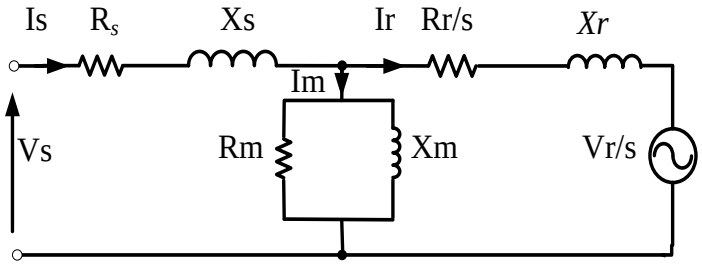

Figure 2. DFIG's per-phase equivalent model for steady-state operation

The matrix form of the equation for this circuit is:

$$\begin{bmatrix} V_s \\ \frac{V_r}{s} \end{bmatrix} = \begin{bmatrix} R_s + j(X_s + X_m) & -jX_m \\ -jX_m & \frac{R_r}{s} + j(X_s + X_m) \end{bmatrix} \begin{bmatrix} I_s \\ I_r \end{bmatrix} \quad (1)$$

The frequency relationship for the DFIG can be developed as follows [7]:

$$f_s = f_m + f_r \quad (2)$$

where f_s is the frequency of the stator voltage, f_m is the frequency of the rotating shaft and f_r is the frequency of the injected rotor voltage. The stator voltage and rotor voltage relationship, neglecting the voltage drops in the series elements can be expressed as:

$$|V_s| = \frac{|V_r'|}{s} \quad (3)$$

where the frequency of the rotor voltage is given by:

$$f_r = sf_s$$

The injected rotor voltage and the stator voltage has a ratio *a* given by:

$$a = \frac{n_s}{n_r} = \frac{V_r^{'}}{V_r} \tag{4}$$

where n_s and n_r are the turns of the stator windings and the rotor windings, $V_r^{'}$ is the rotor voltage seen at the stator side and V_r is the rotor voltage. Induced stator voltage can be obtained by substituting value of $V_r^{'}$ from (4) in (3) [8]-[9].

$$V_s = a.\frac{V_r}{s}$$

3. Operation of GSC with VOC and reactive power control

In order to analyze GSC, Figure 1 is reduced by replacing the wind turbine, DFIG and RSC by a battery in series with a small resistance that represents the power losses in the system as shown in Figure 3 [10]-[11].

3.1. Voltage oriented control (VOC)

GSC is controlled by the voltage oriented contro l(VOC) scheme [8-12] as shown in Figure 3. Assuming the three-phase balanced sinusoidal grid voltages v_{ag}, v_{bg} and v_{cg} are in the *abc* stationary reference frame given by:

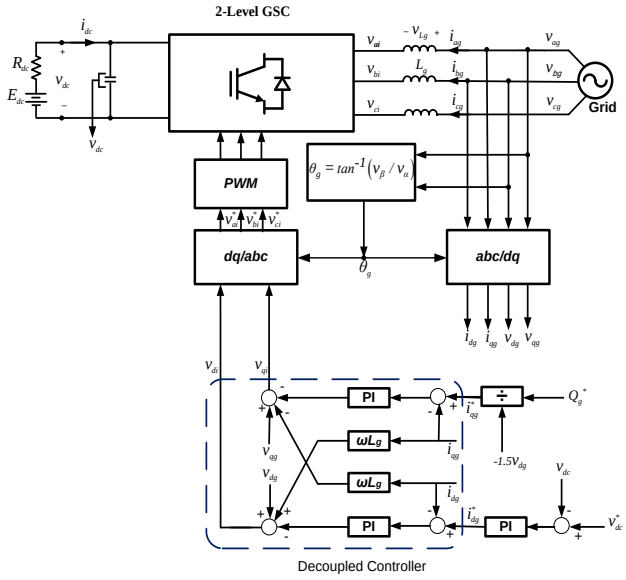

Figure 3. Voltage oriented Control (VOC) with a decoupled controller

$$\left.\begin{aligned} v_{ag} &= v_g \cos\theta_g \\ v_{bg} &= v_g \cos(\theta_g - 120°) \\ v_{bg} &= v_g \cos(\theta_g - 240°) \end{aligned}\right\} \text{ for } (v_{ag} + v_{bg} + v_{bg}) = 0$$

Then θ_g can be detected by: $\theta_g = \tan^{-1}\left(v_\beta \div v\alpha\right)$

where v_α and v_β are obtained by the *abc/αβ* transformation:

$$\begin{bmatrix} v_\alpha(t) \\ v_\beta(t) \end{bmatrix} = \frac{2}{3}\begin{bmatrix} 1 & -\frac{1}{2} & -\frac{1}{2} \\ 0 & \frac{\sqrt{3}}{2} & -\frac{\sqrt{3}}{2} \end{bmatrix}\begin{bmatrix} v_{ag}(t) \\ v_{bg}(t) \\ v_{cg}(t) \end{bmatrix} \quad (5)$$

There are two inner current loops for the accurate control of the *dq*-axis currents i_{dg} and i_{qg}, and one outer dc voltage feedback loop for the control of dc voltage v_{dc}. With the VOC scheme, the three-phase line currents in the *abc*stationary frame i_{ag}, i_{bg} and i_{cg} are transformed to the two-phase currents i_{dg} and i_{qg} in the *dq*synchronous frame, which are the active and reactive components of the three-phase line currents, respectively. In VOC control scheme, the *q*-axis grid voltage v_{qg} is zero $\left(v_{qg} = \sqrt{v_g^2 - v_{dg}^2} = 0\right)$ while *d*-axis grid voltage v_{dg} is equal to v_g $\left(v_{dg} = v_g\right)$, from which the active and reactive power of the system can be calculated by:

$$\left.\begin{aligned} P_g &= \frac{3}{2}\left(v_{dg}i_{dg} + v_{qg}i_{qg}\right) = \frac{3}{2}v_{dg}i_{dg} \\ Q_g &= \frac{3}{2}\left(v_{qg}i_{dg} - v_{dg}i_{qg}\right) = -\frac{3}{2}v_{dg}i_{qg} \end{aligned}\right\} \quad \text{for } v_{qg} = 0$$

The *q*-axis current reference i_{qg}^* can then be obtained from:

$$i_{qg}^* = \frac{Q_g^*}{-1.5v_{dg}}$$

where Q_g^* is the reference for the reactive power, set to zero for unity power factor operation, and a negative value for leading power factor operation.The*d*-axis current reference i_{dg}^*, which represents the active power of the system, is generated by the PI controller for dc voltage control. When the inverter operates in steady state, the dc voltage v_{dc} of the inverter is kept constant at a value set by its reference voltage v_{dc}^*. The PI controller generates the reference current i_{dg}^* according to the operating conditions. Hence, the active power on the ac side of the GSC is equal to the dc-side power (neglecting the losses in the GSC), that is,

$$P_g = 1.5v_{dg}i_{dg} = v_{dc}i_{dc}$$

3.2. VOC with decoupled controller

The state equation for GSC in the *dq*synchronous reference frame can be expressed as [8]:

$$\begin{bmatrix} \frac{di_{dg}}{dt} = \left(v_{dg} - v_{di} + \omega_g L_g i_{qg}\right)/L_g \\ \frac{di_{qg}}{dt} = \left(v_{qg} - v_{qi} + \omega_g L_g i_{dg}\right)/L_g \end{bmatrix} \quad (6)$$

Equation (6) illustrates that the system control is “cross-coupled”. The output of the Decoupled PI Controller can be expressed as:

$$\begin{bmatrix} v_{di} = -\left(k_1 + k_2 / S\right)\left(i_{dg}^{*} - i_{dg}\right) + \omega_g L_g i_{qg} + v_{dg} \\ v_{qi} = -\left(k_1 + k_2 / S\right)\left(i_{qg}^{*} - i_{qg}\right) - \omega_g L_g i_{dg} + v_{qg} \end{bmatrix} \quad (7)$$

where (*k1 + k2 /S*) is the transfer function of the PI controller. Substituting (7) into (6) yields:

$$\begin{bmatrix} \frac{di_{dg}}{dt} = \left(k_1 + k_2 / S\right)\left(i_{dg}^{*} - i_{dg}\right) / L_g \\ \frac{di_{qg}}{dt} = \left(k_1 + k_2 / S\right)\left(i_{qg}^{*} - i_{qg}\right) / L_g \end{bmatrix}$$

The above equation indicates that the control of the d-axis grid current i_{dg} is decoupled, involving only d-axis components, so is the q-axis current i_{qg}. The decoupled control makes the design of the PI controllers more convenient, and system is easier to be stabilized.

4. Space vector modulation for GSC

Space vector modulation (SVM) is one of the real-time modulation techniques and is widely used for digital control of voltage source inverter [13]-[14].

5. Simulation results

Consider a 2.3MW/690V GSC, controlled by the VOC scheme with a decoupled PI controller as shown in Figure 3. The system parameters and operating conditions are given in Table 1.

Table 1. Simulation Parameters

Parameters	Symbols	Ratings	Per unit values
Dc Resistance	R_{dc}	0.0207Ω	0.1
Battery voltage	*E*	1259 V	3.16
Grid-side filter inductor	L_{grid}	0.1098mH	0.2
Dc reference voltage	v_{dc} *	1220V	3.062
modulation index	m_a	0.8	---

Figure 4 shows the waveforms of the phase-*a* grid voltage v_{ag} and the space angle θ_g. When v_g rotates in space, θ_g and v_{ag} varies from zero to 2*π* periodically. When θ_g is equal to zero, v_{dg} reaches its peak value as shown at Point *A* in Figure 4.

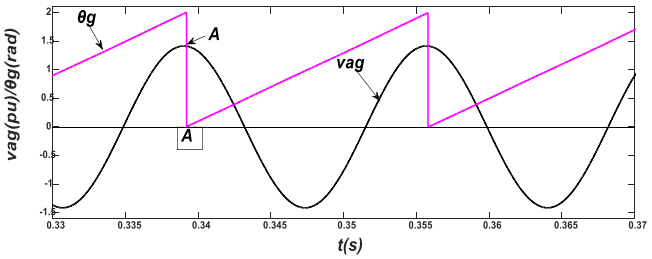

Figure 4. Angle of grid voltage vector for the voc scheme

The transient waveforms of the inverter are illustrated in Figure 5, where the inverter initially delivers the rated active power $(P_g = -1p.u)$ and zero reactive power $(Q_g = 0p.u)$ to the grid. Ignoring all the ripples (produced by current harmonics), the *d*-axis current i_{dg} is -1.41pu (rated) and the zero *q*-axis current i_{qg} is zero. The corresponding waveforms of phase-*a* grid voltage and current during the transient are also given in the Figure 6.

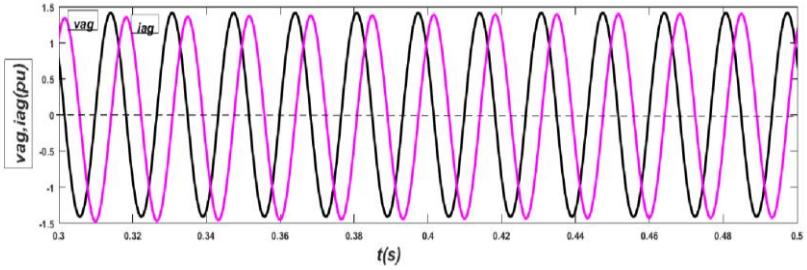

Figure 5. transient waveforms of the grid-tied inverter with voltage oriented control

Figure 6 shows the peak value of the phase-a grid current $i_{ag}$is equal to the peak value of the phase-a grid voltage v_{ag} *i.e*1.414 pu (rated).The grid current i_{ag} is out of phase with its voltage v_{ag} by 180° so both the active and reactive powers delivered to the grid can be calculated as:

$$P_g = V_{ag} I_{ag} \cos\phi_g = \frac{1}{2}(1.414 \times 1.414) \times \cos 180° = -1pu$$

$$Q_g = V_{ag} I_{ag} \sin\phi_g = \frac{1}{2}(1.414 \times 1.414) \times \sin 180° = 0\,pu$$

Where the negative sign indicates that the GSC delivers the active power to the grid.

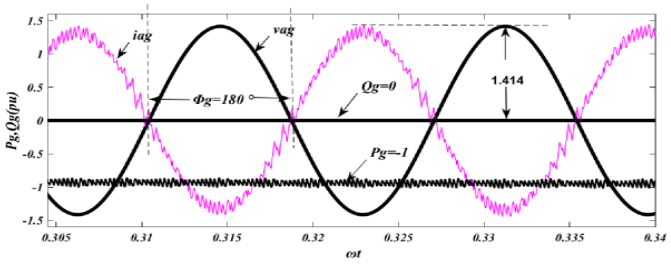

Figure 6. Steady-state operation-I

Figure 7 depicts, when the battery voltage E starts to reduce such that the active power to the grid P_g is reduced to -0.8pu, which leads the reduction of the d-axis current i_{dg} from its rated value to -1.13pu *(√2 ×-0.8)*. The q-axis current i_{qg} remains unchanged during the transients due to the decoupled control of the active and reactive power while the magnitude of the phase-a grid current i_{ag} is reduced to 1.33pu, but kept out of phase with its voltage by 216.87°. Both the active and reactive powers to the grid can be calculated by:

$$P_g = V_{ag} I_{ag} \cos\phi_g = \frac{1}{2}(1.33 \times 1.414) \times \cos 216.87° = -0.8\,pu$$

$$Q_g = V_{ag} I_{ag} \sin\phi_g = \frac{1}{2}(1.33 \times 1.414) \times \sin 216.87° = -0.6\,pu$$

The negative reactive power indicates that the GSC operated with leading (capacitive) power factor to sustain the grid voltage.

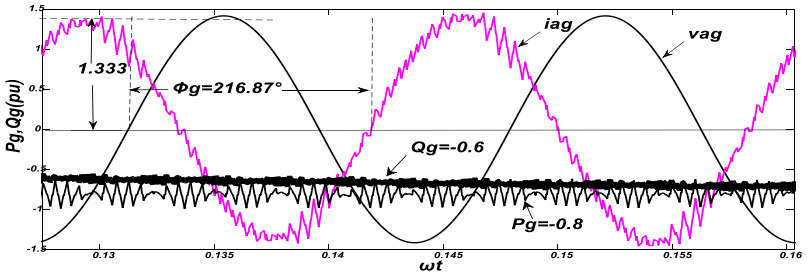

Figure 7. Steady-state operation-II

6. Conclusion

GSC is controlled by Voltage Oriented Control (VOC) scheme with a decoupled PI controller. It successfully kept the dc link voltage v_{dc} constant and provided reactive power to the grid in leading power factor.

References

[1] W Cao, Y Xie, Z Tan. Wind Turbine Generator Technologies, intechopen. Chapter 7. 2012: 177-204. [Online]. Available: http://cdn.intechopen.com/pdfs-wm/38933.pdf.
[2] Junio S Bulhoes, Geovanne P Furriel et al. *Parametric regression in synchronous and induction generators.* IEEE Conference publication, 18th International Scientific Conference on Electric Power Engineering (EPE), 2017.
[3] Kong Lingming, He Yufei. *Study on the control strategy for oscillatory stability enhancement using DF IG wind turbine system.* IEEE Conferencepublication, 4th International Conferenceon Industrial Engin eering and Applications (ICIEA). 2017.
[4] Masters thesis of X Jing. Modeling and Control of a Doubly-Fed Induction Generator for Wind Turbine Generator Systems. Submitted to Faculty of the Graduate School, Marquette University. 2012.
[5] Ahmed A Zaki Diab, Salah A Abdel Maksoud et al. *Performance of doubly-fed induction generator bas ed wind turbine using adaptive neuro-fuzzy inference system*. IEEE Conference Publication,11th Inter national ForumonStrategicTechnology (IFOST). 2016.
[6] Andrii Chub, Dmitri Vinnikov et al. Wide Input Voltage Range Photovoltaic Microconverter with Reconfigurable Buck–Boost Switching Stage. *IEEE Transactions on Industrial Electronics*. 2017; 64(7): 5974-5983.
[7] L Fan, SYuvarajan. *Modeling and slip control of a doubly fed induction wind turbine generator*. IEEE Power Symposium, NAPS '08. 40th North American, Calgary. 2008: 1-6.
[8] Paul C Krause, Oleg Wasynczuk, Scott D. Sudhoff. *Analysis of Electric Machinery and Drive Systems*. Wiley-IEEE Press; 2 edition. 2002. ISBN: 978-0471143260.
[9] BK Bose. Modern Power Electronics and AC Drives. Prentice Hall. 2001.
[10] B Wu. Power Conversion and Control of Wind Energy Systems. Wiley-IEEE Press. 2011.
[11] V Akhmatov. Induction Generators for Wind Power. Multi-Science Publishing Co. Ltd. Press. 2005.
[12] E Tremblay, A Chandra, PJ Lagace. Grid-side converter control of DFIG wind turbines to enhance power quality of distribution network. *IEEE Power Engineering Society General Meeting*. 2006: 06.
[13] J Dai, Y Lang, B Wu, D Xu, NR Zargari. A Multisampling SVM scheme for current source converter wi th Superior Harmonic Performance. I*EEE Transactions on Power Electronics*. 2009; 24(11): 2436-2455.
[14] B Wu. High-Power Converters and AC Drives. Wiley-IEEE Press. 2006.